

# Application of GS-MOCSO Algorithm to Slow-wave Structure Design of STWT

Dongming Zhao, Kewen Xia, Huijuan Liu and Xiaoxu Shi

**Abstract**— A space travelling wave tube (STWT) is an important microwave device that serves as the final-stage power amplifier in satellite systems and performs high-power signal conversion. The focus of this paper is the multi-objective problem of improving the electronic beam efficiency and suppressing nonlinear distortion for the slow-wave structure design of the STWT. We propose a design method based on multi-objective cat swarm optimization with gravitational search operator (GS-MOCSO) to improve the slow-wave structure. Electron beam efficiency and phase shift are used as the two objective functions, and 1-D CHRISTINE code is introduced to obtain the output value of the STWT. Finally, the best pitch distribution can be calculated by GS-MOCSO. An experiment is conducted based on GS-MOCSO, and the traditional multi-objective cat swarm optimization (MOCSO) is introduced for a baseline performance comparison. The experimental results demonstrate that the electronic beam efficiency on the best pitch distribution obtained by GS-MOCSO reaches 40.2%, which is 10.2% higher than the rated value of 30%. Moreover, it is higher than the value achieved by MOCSO, which reaches only 38.5%. Then, the phase shift is only  $36.5^\circ$ , which is a reduction of  $23.5^\circ$  compared to the value  $60^\circ$  under a constant pitch. Extensive investigations were also performed on the varying trends of beam efficiency and phase shift using input power scanning. The proposed method is highly suitable for the slow-wave structure design of STWT, and the GS-MOCSO algorithm is superior to the MOCSO algorithm for the multi-objective problem (MOP) of beam efficiency and phase shift.

**Index Terms**— space traveling-wave tube, slow-wave structure, multi-objective problem, cat swarm optimization, gravitational search operator

## I. INTRODUCTION

A travelling-wave tube (TWT) is a microwave device that amplifies an electromagnetic wave travelling along a slow-wave structure. TWTs are important microwave devices that are widely used in radar, electronic warfare, communications and other fields. A space travelling-wave tube (STWT) is a special type of

travelling-wave tube used in the space technology field; it serves as the final-stage power amplifier in satellite systems to perform high-power signal conversions. The STWT is the research target of this paper. An STWT is a critical component in satellite communications, thus, it must exhibit high efficiency, high gain and high linearity; consequently, the STWT manufacturing process must maintain high standards. The power amplification effect of an STWT depends on the interaction between the electron beam and electromagnetic wave, and the speed of the electromagnetic wave along the axial position should be nearly equal to that of the electron beam to achieve energy exchange. The circuit that generates travelling-wave fields along the axis is a slow-wave structure; pitch distribution is one of its core parameters. The primary target of pitch distribution design in a slow-wave structure is to improve the electron beam efficiency and reduce the phase distortion. The electronic beam efficiency and linear amplification characteristics of an STWT are controlled and influenced by each other; therefore, these values need to be solved through a multi-objective problem (MOP) optimization. In recent years, applying swarm intelligence optimization methods to solve MOPs has become a hot topic. The optimum pitch distribution is obtained through simulations to ensure both high electronic beam efficiency and small phase distortion. The slow-wave structure of an STWT can be designed contrapuntally to reduce the difficulty of this work.

It is difficult to simultaneously improve the electronic beam efficiency and suppress nonlinear distortion for the slow-wave structure design of an STWT [1]–[2]. Previously published research studies have examined the effects of slow-wave structure parameters (i.e., length and pitch) on electron beam efficiency and gain, and some valuable results were obtained in [3]–[5]. In our previous paper, a new swarm intelligence algorithm, called quantum particle swarm optimization (QPSO) [6], was introduced to optimize the slow-wave structure of a TWT with 1-D CHRISTINE code and applied to find the optimal pitch distribution as in [7]. However, QPSO's convergence speed and efficiency improvement are unsatisfactory; therefore, a new intelligence algorithm should be developed to optimize the STWT slow-wave structure and obtain the best pitch distribution to maximize the electron beam efficiency. The cat swarm optimization (CSO) [8] is a recently developed intelligent algorithm based on swarm intelligence that imitates the natural behaviour of cats. The CSO has achieved excellent optimization results in many fields [9]–[13]. In recent years, scholars have focused on applying multi-objective PSO and multi-objective CSO algorithms to solve MOP problems, with excellent results, as detailed in [14]–[18]. To avoid

Manuscript received May 06, 2017, revised Oct 30, 2017. This work was supported by the Natural Science Foundation of Hebei Province (Grant No. E2016202341) and Research Project of Science and Technology for Hebei Province Higher Education Institutions (Grant No.BJ2014013).

Dongming Zhao is with the School of Electronic Information Engineering, Hebei University of Technology, Tianjin, 300401, PR China. (E-mail: waitman\_840602@163.com)

Kewen Xia, is with the School of Electronic Information Engineering, Hebei University of Technology, Tianjin, 300401, PR China. (E-mail: kwxia@hebut.edu.cn)

Huijuan Liu is with Tianjin Broadcasting TV and Film Institute, Tianjin, 300112, PR China. (E-mail: liuhuijuan1110@163.com).

Xiaoxu Shi is with the School of Electronic Information Engineering, Hebei University of Technology, Tianjin, 300401, PR China. (E-mail: sxx\_0909@163.com).

premature convergence and local optimum results, the gravity search operator derived from the gravity search algorithm is applied to improve the population diversity and obtain a high -precision solution, as in [19]–[20]. In addition, some new swarm intelligence algorithms [21]–[22] are also helpful for the algorithm research in this paper.

The remainder of this paper is organized as follows. Section II introduces the pitch distribution optimization in the slow-wave structure and the 1-D CHRISTINE code. In Section III, a new GS-MOCSO is proposed such that each cat's position is influenced by the gravitational force of the optimum cats, which generates a better population in the next iteration and helps avoid local optimum results. Section IV proposes applying the GS-MOCSO application flow to slow-wave structure design. To obtain the best pitch distribution, GS-MOCSO is used to solve the MOP to improve the electronic beam efficiency and suppress phase distortion. Section V presents an experimental analysis and discussion concerning the application of GS-MOCSO to slow-wave structure design. Electronic beam efficiency and phase shift are set as the two objective functions, and the GS-MOCSO is compared to MOCSO regarding multi-objective optimization performance and the change trend of pitch distribution. Finally, in Section VI, some conclusions are drawn.

## II. SLOW-WAVE STRUCTURE DESIGN

The primary objective of pitch distribution optimization in the slow-wave structure design of STWT is to achieve higher electronic beam efficiency and lower nonlinear phase shift. The influence mechanism of pitch distribution on the beam-wave interaction of slow-wave structure is explained in detail in the chapter, and the calculation process of 1-D CHRISTINE code is also given.

### A. Pitch distribution in slow-wave structure

The STWT studied in this paper is a helix traveling-wave tube. Fig 1 shows a diagram of helix slow-wave structure in a STWT. In the slow-wave structure, the electromagnetic wave velocity is kept synchronized with the electron beam velocity to generate interaction and energy exchange between them, and it is reduced and becomes practically equal to the electron beam velocity through the pitch variation in the slow-wave structure. During this process, the electromagnetic wave can be amplified in the interaction region and its energy is transferred to electron beam.

In the axial direction, it can also be divided into the following sections: input section  $L_0$  (length  $l_0$ , pitch  $P_0$ ), phase velocity increase section  $L_1$  (length  $l_1$ , pitch  $P_1$ ), phase velocity decrease section  $L_2$  (length  $l_2$ , pitch  $P_2$ ). In the  $L_1$  section, phase compensation and effective electron beam bunching can be completed, in the  $L_2$  section, as much bunching electron beam energy as possible is transferred to the high frequency field to improve the electronic beam efficiency of the STWT. During the electron beam bunching process, nonlinear distortion began to appear, the harmonic distortion arises from the incentive function of harmonic current generated by bunching process in the slow-wave structure, and reflection effect in the slow-wave structure generate intermodulation distortion. A set of pitch values  $\{P_0, P_1, P_2\}$

form a pitch distribution, that directly determines the energy exchange efficiency between the electron beam and electromagnetic wave. The gradient or jump change in the pitch is an effective to realize phase velocity resynchronization, and it is also the most frequently used slow-wave structure of a STWT to improve electronic beam efficiency and suppress nonlinear phase distortion. The paper is to study the best pitch distribution along the axis in the interaction region of STWT.

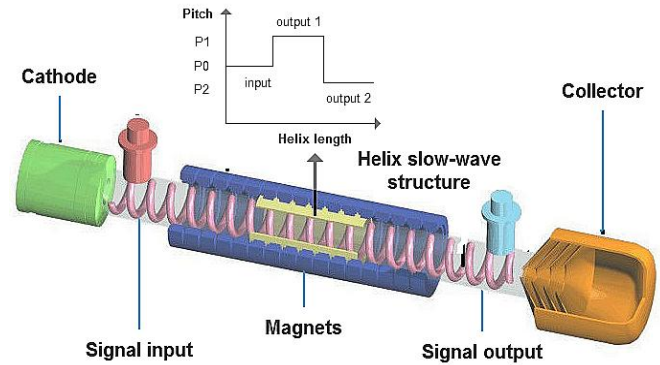


Fig 1. Diagram of helix slow-wave structure in a STWT

### B. Calculation process of 1-D CHRISTINE code

In this paper, 1-D CHRISTINE code as in [5] is used for theoretical analysis and numerical simulation of slow-wave structure. The basic equations of 1-D nonlinear beam-wave interaction in STWT are expressed as:

The field equations of nonlinear theory can be expressed as:

$$\left( \frac{d}{dz} + \alpha_n(z) \right) a_n(z) = \frac{2\pi i}{I_A} I e_2^*(n, z) \langle e^{-i\psi_n} \rangle \quad (1)$$

Phase change rate of electric ring along axial direction is:

$$\frac{d\psi_n}{dz} = \omega_n (1/v_{z0} - 1/v_z) \quad (2)$$

An equation of electronic longitudinal motion is:

$$\frac{d\gamma}{dz} \Big|_{rf} = \text{Re} \left\{ 2i \sum_n a_n(z) \cdot e_2(n, z) e^{i\psi_n} - \frac{8Ii}{I_a (r_{bo}^2 - r_{bi}^2)} \sum_n \frac{cR'_n}{\omega_n} e^{i\psi_n} \langle e^{-i\psi_n} \rangle \right\} + \frac{q}{mc^2} \langle z \cdot E_{dc} \rangle_{beam} \quad (3)$$

And the normalized field amplitude is

$$\alpha_n = - \frac{1}{2A_{eff,n}} \frac{\partial A_{eff,n}}{\partial z} \quad (4)$$

The normalized total field is:

$$e_2(n, z) = \left( \langle z * e_n \rangle_{beam} / A_{eff,n}^{1/2} \right) * \exp \left[ i \int_0^z (k_{zn}(z') - \omega_n / v_{z0}) dz' \right] \quad (5)$$

The space step integration method is usually used to solve the Eq. (1) - (3), the iterative computation is executed using the 4th-order Runge-Kutta method. The output parameters of the STWT such as output power, phase shift, gain, beam efficiency, can be calculated by the 1-D CHRISTINE code under the conditions of suitable normalized complex amplitude, electron phase and relativistic factor.

The output power  $P$  of the normalized complex amplitude in electromagnetic field  $a_n(z)$  is as follows:

$$P = P_{flux,2} \sum_n |a_n(z)|^2, P_{flux,2} = 1.386 * 10^9 W \quad (6)$$

The gain  $G$  is defined as:

$$G = 10 * \lg(P/P_{in}) \quad (7)$$

Electronic beam efficiency  $\eta_{eff}$  is defined as

$$\eta_{eff}(\lambda, P_m) = \frac{P_{out}(x_i) - P_{in}}{P_e} = \frac{P_{out}(x_i) - P_{in}}{I_b V_b} \quad (8)$$

TABLE I  
PHYSICAL PARAMETER INTERPRETATION

Function	Expression
$I_A$	Current constant ( $1.7 * 10^4$ A)
$k_{zn}$	The longitudinal propagation constant of the $n$ th harmonic
$e_n(x)$	The $n$ th normalized harmonic of the field
$\varphi_n$	Electron phase
$\gamma$	Relativistic factor
$v_{z0}$	The initial axial velocity
$n$	Harmonic number of the field
$n'$	the harmonic number in the AC space charge field
$r_{bo}$	Inner radii of the electron beam
$r_{bi}$	Outer radii of the electron beam
$P_{out}$	RF output power
$P_{in}$	RF input power
$P_e$	Electron beam power
$I_b$	Current of the electron beam
$V_b$	Voltage of the electron beam
$x_i$	Helix pitch value
$\lambda$	A pitch distribution (a set of pitch values)

### III. AN INNOVATIVE MULTI-OBJECTIVE CAT SWARM OPTIMIZATION ALGORITHM

The simultaneous electronic efficiency improvement and nonlinear distortion suppression of STWT need to be solved by multi-objective optimization. The excellent performance of multi-objective cat swarm optimization algorithm (MOCSO) has been demonstrated for various optimization problems. This paper proposes a innovative MOCSO algorithm with gravitational search operator, and several optimization problems are tested to demonstrate its superiority compared to existing algorithms.

#### A. Multi-objective problem

Multi-objective problem is composed of the variable vector  $X$ , the vector objective function  $Y$  and a set of constraints, the model is defined as:

$$\begin{aligned} \min y &= F(x) = (f_1(x), f_2(x), \dots, f_k(x)) \\ x \in S &= \{x | g_i(x) \leq 0, i = 1, 2, \dots, m\} \\ x &= (x_1, x_2, \dots, x_n) \in X, \quad y = (y_1, y_2, \dots, y_k) \in Y \\ X &= \{(x_1, x_2, \dots, x_n) | l_i \leq x_i \leq u_i, i = 1, 2, \dots, n\} \\ L &= (l_1, l_2, \dots, l_n), \quad U = (u_1, u_2, \dots, u_n) \end{aligned} \quad (9)$$

For vectors  $u = (u_1, u_2, \dots, u_k)$  &  $v = (v_1, v_2, \dots, v_k)$ , the vector  $f(u_i)$  dominates vector  $f(v_i)$  if and only if,

$$\begin{cases} f(u_i) \leq f(v_i), \forall i \in \{1, 2, \dots, k\} \\ f(u_i) < f(v_i), \exists i \in \{1, 2, \dots, k\} \end{cases} \quad (10)$$

When  $u$  performs better than  $v$  for at least one objective, we define that solution  $u$  dominates  $v$ . The notation  $x^* \in X$  indicates that when solution  $x^*$  is not dominated by any other solutions, a Pareto-optimal solution is obtained in  $X$ . The curve containing all the Pareto-optimal solutions is defined as Pareto-optimal front. The solutions on a Pareto-optimal front are called non-dominated solutions. The various objective functions in MOP are not directly comparable and may not conflict with each other, so the MOP has no just one optimal solution for all objective-functions, but has a set of solutions called the "Pareto-optimal solution set".

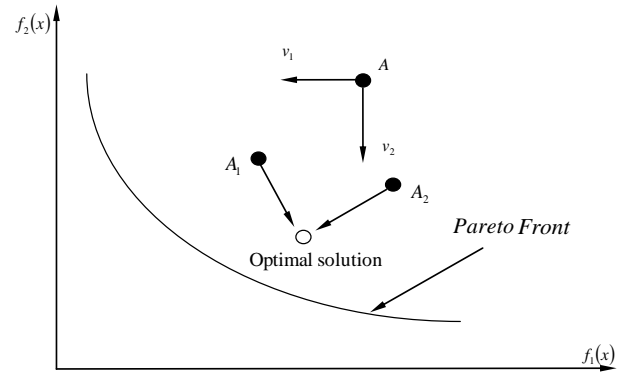


Fig 2. Schematic diagram of the objective function space particles trend and Pareto front

#### B. Multi-objective cat swarm optimization (MOCSO)

The cat swarm optimization method was proposed by Chu and Tsai [8] and imitates the constant attentive behaviour of cats. Even at rest, cats remain alert so they can hunt and catch moving prey, and cats move slowly when seeking potential hunting opportunities. This behaviour is termed "seeking mode". After locking onto prey, cats increase their speed and may use much energy to capture it. This behaviour is termed "tracing mode". Seeking mode enhances the global search capability, whereas tracing mode enhances the search accuracy to perform efficient local searches. Cats are distributed to prey according to a mixture ratio ( $MR$ ). The steps of the MOCSO algorithm are as follows.

1. The solution space is  $d$ -dimensional ( $I < d < D$ ). The positions of cats are randomly initialized in  $d$ -dimensional space, where  $x_{i,d}$  is the position of the  $i$ -th cat in the  $d$ -th dimension.
2. Initialize the velocity of cats, where  $v_{i,d}$  is the velocity of the  $i$ -th cat.
3. Randomly assign cats to either seeking mode or tracing mode based on the  $MR$ .
4. Evaluate all cats' fitness values.
5. Store the cats' positions (the Pareto-optimal solutions) in an archive.
6. If the algorithm's termination conditions are satisfied, terminate the algorithm; otherwise, repeat steps 3 to 5.

### C. GS-MOCSO algorithm

The mechanism of CSO algorithm generating population position does not fully consider the position information of other optimum cats, so it's hard to adequately guarantee the diversity of the cats. When the best position is not at or near the starting point, the CSO result may not be sufficiently ideal and may gradually fall into a local optimum point. In this paper, we introduce a universal gravitation search operator to increase the diversity of the cats and improve the global optimization capability. A MOCSO with gravitational search operator (GS-MOCSO) algorithm is proposed in which the position of each cat is influenced by the gravitational forces of the other optimum cats, thus generating a better population in the next iteration to avoid premature convergence and local optimums.

#### Linear MR

The global search range can be improved by increasing the ratio of seeking cats in early stages. An increase in the ratio of tracing cats will improve the local search accuracy and guarantee the convergence of the algorithm in later stages. The expression determining the search mode distribution of cats based on linear mixture ratio  $MR_L$  is as follows:

$$MR_L = MR_{max} - (MR_{max} - MR_{min}) * \frac{t}{IT_{max}} \quad (11)$$

Where  $MR_{max}$  and  $MR_{min}$  are the highest and the lowest values of mixture ratios,  $t$  is the current iteration number, and  $IT_{max}$  is the maximum iteration number.  $MR_L$  can dynamically adjust the cat mode distribution to optimize the values of  $MR$ .

#### Seeking Mode (SM)

In seeking mode, a cat constantly moves toward its next position. Four parameters used to define this mode: the probability of a mutation operation (PMO), the counts of dimensions to change (CDC), The seeking memory pool (SMP), and the seeking range of the selected dimension (SRD).

Step 1. Based on the SMP, K copies of the  $i$ -th cat are generated.

Step 2. The CDC is produced for every cat; thus, a population of cats is generated. For the entire cat swarm, a mutation is performed according to the SRD.

Step 3. Evaluate the fitness of all K copies.

Step 4. Nondominated selections are used to define the nondominated cat positions on the basis of their fitness values. The nondominated cat positions are stored in an external archive.

Step 5. Replace the current position of cat <sub>$i$</sub>  with the optimum solution in the SMP.

#### Tracing Mode (TM)

In tracing mode, cats change their positions quickly to pursue their prey. The next movement direction of each cat is determined based on the cat's velocity and the best position in the cat swarm.

We define the  $i$ th cat position as  $x_{i,d}$  and the velocity of the  $i$ th cat as  $v_{i,d}$ , where  $x_{i,d} = (x_{i,1}, x_{i,2}, x_{i,3}, \dots, x_{i,D})$  and

$v_{i,d} = (v_{i,1}, v_{i,2}, v_{i,3}, \dots, v_{i,D})$ . The global best position  $x_{g,d}$  of the cat swarm is denoted as  $x_{g,d} = (x_{g,1}, x_{g,2}, x_{g,3}, \dots, x_{g,D})$ .

According to the status (seek or trace) of each cat, the mathematical model of the tracing mode is established as follows:

Step1. The solution space is  $d$ -dimensional ( $1 < d < D$ ). Compute the new velocity of the  $i$ th cat. The velocity of the  $i$ th cat in every dimension is updated by

$$v_{i,d} = w * v_{i,d} + c * r * (x_{g,d} - x_{i,d}) \quad (12)$$

Where  $w$  is inertial weight,  $c$  is acceleration constant and  $r$  is a random number in  $[0, 1]$ . The initial global best  $x_{g,d}$  is selected randomly from the external archive.

Step2. Compute the new position of the  $i$ th cat.

$$x_{i,d}^n = x_{i,d} + v_{i,d} \quad (13)$$

Step3. If the new position of the  $i$ th cat in any dimension is out of the search space range, the velocity of the current dimension is set to the boundary value and is multiplied by -1 to the reverse search direction.

Step4. Evaluate the fitness of all cats.

Step5. The external archive is updated by new positions which represent nondominated solutions.

#### Gravitational Search Process

Gravity search operator is introduced into MOCSO in this paper. The dimension information of cats can be changed by applying the displacement operation according to interactions and gravitational forces between cats. The nondominated optimal solutions information in external archive is shared in the whole population to ensure that every cat improves a poor dimension value. The set of all cats' new positions updated by gravity is generated as the initial population in the next iteration.

The gravitational and inertial masses are expressed by the following Eq. (14) - (15):

$$m_{i,d} = \frac{f(x_{i,d}) - \max_{x_{j,d} \in w(t)} f(x_{j,d})}{\min_{x_{j,d} \in w(t)} f(x_{j,d}) - \max_{x_{j,d} \in w(t)} f(x_{j,d})} \quad (14)$$

$$M_{i,d} = \frac{m_{i,d}}{\sum_{x_{j,d} \in w(t)} m_{j,d}} \quad (15)$$

Gravitational and inertial masses are calculated using the fitness evaluation. A heavier mass means a better cat, meaning that better cats have greater attraction and move more slowly.  $f[X(t)]$  represents the fitness value of cat  $X(t)$  at time  $t$ , and  $W(t)$  is the aggregation of  $N$  cats  $X(t)$  at time  $t$ . The set of all cats is  $N_a$ , and the  $i, j$  cat position is  $x_{i,d}, x_{j,d}$  ( $1 < d < D$ ). The first  $2*N$  cats of greatest mass from  $N_a$  (small fitness value) are selected to form the optimum cats ( $R$ ) used as the attractive element to exert a gravitational effect on  $W(t)$ . The gravity is defined as:

$$F_{i,d} = \sum_{j \in R, j \neq i} rand(0,1) * F_{i,j,d} \quad (15)$$

$$F_{i,j,d} = G \frac{M_i * M_j}{r_{i,j} + \epsilon} (x_{j,d} - x_{i,d}) \quad (16)$$

Where  $F_{i,d}$  is the sum of the forces on the  $i$ th cat in the  $d$ -dimensional space,  $G$  is the gravitational constant,  $M_i$  is the passive inertial mass related to the  $i$ th cat,  $r_{i,j}$  is the Euclidean distance between the  $i$ th and  $j$ th cats, and  $\epsilon$  is a small constant. Under gravity  $F_{i,d}$ , the  $i$ th cat  $x_{i,d}$  exhibits a position change in each dimension, and new position  $x'_{i,d}$  is express as:

$$x'_{i,d} = x_{i,d} + F_{i,d} / M_i \quad (17)$$

$V(t) = (x'_1, x'_2, x'_3, \dots, x'_i)$  is the set of all cats' new positions updated by gravity. According to the fitness value,  $N$  cats are selected from the set  $\{W(t) \cup V(t)\}$  and set as the initial population  $X(t+1)$  in the next iteration.

Based on the gravitational action of  $2*N$  cat with the best fitness values, the poor positions information of other cats can interact with optimum cats (nondominated optimal solutions) in each dimension to increase the diversity of cats and prevent falling into local optimum. The schematic diagram of GS- MOCSSO algorithm is shown in Fig 3.

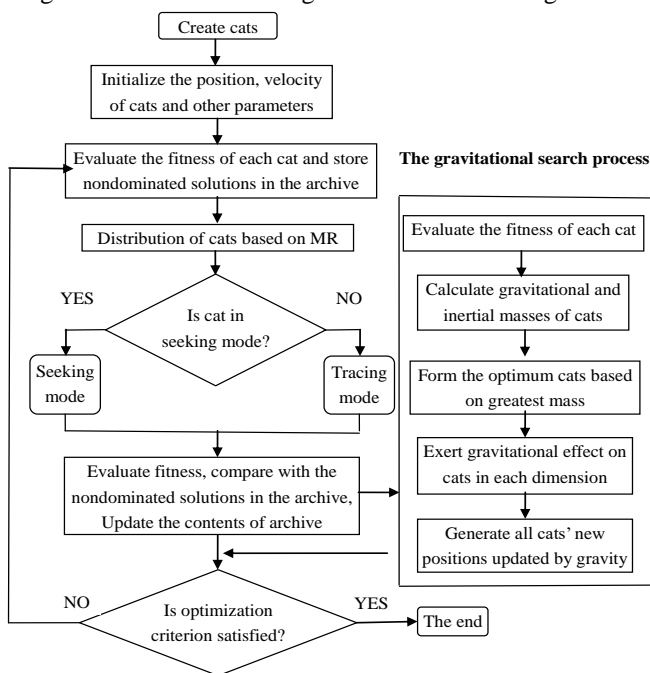


Fig 3. Schematic diagram of GS-MOCSSO algorithm

#### D. Simulation test of algorithms

According to the proposed GS-MOCSSO algorithm, each cat can appear in an arbitrary position in the solution area, and the entire population will be scattered within the area of the solution set. The evaluation of the nondominated optimal solution avoids becoming stuck in the best position of one objective function. More importantly, it reflects the constraint relationship among the multi-objective functions. Some simulation experiments were implemented in MATLAB to demonstrate the performance of GS-MOCSSO for this complex multi-objective problem. The performance

of GS-MOCSSO is validated compared to MOCSSO and MOPSO using the results obtained from four standard test functions, as shown in Table I. The Pareto fronts calculated by the GS-MOCSSO, MOCSSO and MOPSO algorithms for test functions 1~4 are shown in Table II.

The initialization parameters for MOPSO are as follows: archive size = 100, inertia weight = 0.25, acceleration constant = 2, random number is in [0, 1]. The initialization parameters for GS-MOCSSO and MOCSSO are as follows: SMP = 3, SRD = 0.1, CDC = 80%, MR = 0.5, MR<sub>max</sub> = 0.75, MR<sub>min</sub> = 0.25, C = 2, w = 0.5, archive size = 100 and  $r$  is in [0, 1], the maximum iterations = 500. The results obtained from 20 independent simulations are recorded and the best average result is shown on Pareto-front curves in Fig 3.

TABLE II  
TEST FUNCTION EXPRESSIONS

Function	Expression
Test function 1	$\begin{cases} \min f_1 = x^2, \\ \min f_2 = (x-2)^2, x \in [-5,7] \end{cases}$
Test function 2	$\begin{cases} \min f_1(x, y) = (x^2 + y^2)^{\frac{1}{8}}, \\ \min f_2(x, y) = ((x-0.5)^2 + (y-0.5)^2)^{\frac{1}{4}}, x \in [-5,10] \end{cases}$
Test function 3	$\begin{cases} \min f_1 = x_1, \\ \min f_2 = 1 - \left(\frac{f_1}{g}\right)^2, g = 1 + \frac{9}{n-1} \sum_{i=2}^n x_i, n = 30, x_i \in [0,1] \end{cases}$
Test function 4	$\begin{cases} \min f_1(x) = \begin{cases} -x, & \text{if } x \leq 1, \\ -2+x, & \text{if } 1 < x \leq 3, \\ 4-x, & \text{if } 3 < x \leq 4, \\ -4+x, & \text{if } x > 4, \end{cases} \\ \min f_2(x) = (x-5)^2, x \in [-5,10] \end{cases}$

TABLE III  
COMPARISON OF GS-MOCSSO WITH MOCSSO, MOPSO ON ALL THE FOUR TEST FUNCTIONS

Parameter	GS-MOCSSO	CMOCSSO	CMPSO
Test function 1			
$\min f_1$	1.9281	2.5639	2.3916
$\min f_2$	0.3529	0.1590	0.2057
Computation time	1.07315s	1.0665s	1.0452s
Test function 2			
$\min f_1$	0.9005	0.9170	0.9238
$\min f_2$	0.0010	0.0023	0.0031
Computation time	0.09492s	0.097s	0.0887s
Test function 3			
$\min f_1$	0.0000e+248	0.0000e+250	0.0000e+250
$\min f_2$	-1.2365e+248	-7.6602e+250	-2.3713e+250
Computation time	2.4434s	2.3482s	2.1071s
Test function 4			
$\min f_1$	1.5983	0.9965	1.0520
$\min f_2$	1.9375	4.0139	3.7948
Computation time	0.0309s	0.0296s	0.0264s

Test functions 1~4 each contain two objective functions  $f_1(x)$  and  $f_2(x)$  for solving the minimization problem. The cats' positions are initialized and then evaluated by the two

objective functions to obtain Pareto-optimal solutions. As shown in Fig. 4, the solutions are uniformly distributed over the effective surface of the objective functions by iterative computation, the curves are clear and complete, and the results demonstrate the accuracy and reliability of the GS-MOCSO algorithm. GS-MOCSO, MOCSO and MOPSO can all traverse the entire Pareto-front. The GS-MOCSO algorithm performs best in finding the minimum value solution of  $f_1(x)$   $f_2(x)$  except regarding computation time, as shown in Table III.

In MOPSO, the updating process for particle velocity and position is quite approximate in each iteration. Because the seeking and tracing modes must be executed independently, MOCSO requires more computation time than MOPSO. In GS-MOCSO, all the cats' positions are updated at the end of each iteration by the gravitational search operator; then, the new initial population is generated. Hence, GS-MOCSO performs more operations on the cats than do the MOCSO and MOPSO algorithms. Consequently, GS-MOCSO requires more computing time on the test functions than do MOCSO and MOPSO.

#### IV. APPLICATION PROCESS OF GS-MOCSO ALGORITHM FOR SLOW-WAVE STRUCTURE DESIGN

In general, in order to obtain better linear amplification capability, the STWT outputs RF signals before saturation, but this is at the expense of reducing the electronic beam efficiency. The comprehensive processing of the electron beam efficiency and nonlinear phase distortion in slow-wave structure design of STWT is a typical multi-objective problem. The optimization target in this paper is to achieve higher electronic beam efficiency and lower nonlinear phase distortion simultaneously. By setting the electronic beam efficiency and phase shift as the two objective functions, the proposed GS-MOCSO algorithm is used to optimize the slow-wave structure of the helix STWT.

##### A. Mathematical model

The electronic beam efficiency  $\eta_{\text{eff}}$  is defined as the ratio of power difference (between the RF output power  $P_{\text{out}}$  and the RF input power  $P_{\text{in}}$ ) and the electron beam power. The magnitude of phase shift  $Pha(\omega_i)$  represents the degree of nonlinear phase distortion, which indicates that the output phase is affected by the change of input power. A larger phase shift indicates the more serious nonlinear phase distortion. The multi-objective function is defined as follows:

$$\begin{cases} \max f_1(x) = \eta_{\text{eff}}(\lambda, P_m) = \frac{P_{\text{out}}(x) - P_{\text{in}}}{I_b V_b} \\ \min f_2(\omega_i) = Pha(\omega_i) = |\varphi(P_{\text{in}}) - \varphi(P_{\text{in}} - 20\text{dBm})| \end{cases} \quad (18)$$

The multi-objective function has two objective functions,  $f_1(x)$  and  $f_2(\omega_i)$ , which represent electronic beam efficiency  $\eta_{\text{eff}}(\lambda, P_m)$  and phase shift  $Pha(\omega_i)$ , respectively.  $x_{i,d}$  is a helix pitch distribution (a set of pitches), and  $\lambda$  represents various physical parameters that affect the electronic beam efficiency of STWT, such as the radius of the metal vacuum barrel, the average radius of the helix, and the

outside radius of the helix.  $\varphi(P_{\text{in}})$   $\varphi(P_{\text{in}} - 20\text{dBm})$  are the phases obtained for the input power of  $P_{\text{in}}$  and  $P_{\text{in}} - 20\text{dBm}$ , respectively. The difference between them is set as the phase shift  $Pha(\omega_i)$ .

##### B. Experimental parameters

The PC used in the experiment is configured with a 3.8 GHz Intel Core i7 CPU and 8 GB of RAM running MATLAB 2014a. The operating parameters are representative of the base performance of a STWT, such as a 5 GHz operating frequency, 50–52 dBm peak output power, 1 GHz gain bandwidth, 940 gauss Brillouin magnetic field, and electron beam parameters (3,000 v beam voltage, 170 mA beam current, 0.36 mm beam radius, etc.) This study focuses on the pitch distribution in the helix slow-wave structure, which is the most important factor that affects the electronic beam efficiency and phase shift. Our program holds some parameters constant, such as the radius of the metal vacuum barrel (0.2974 cm), the outside radius of the helix (0.13970 cm), the average radius of the helix (0.12446 cm), the helix tape width (0.03556 cm), the electron beam filling rates (0.5), the edge lengths of the support rods (0.0508 × 0.14732 cm), and the clamping rod equivalent relative dielectric constant (1.75 BeO), and so on.

The role of the input section of the slow-wave structure is to focus the electron beam. In an STWT with good beam efficiency, the electron beam delivers maximal energy to the electromagnetic wave in the slow-wave structure, and the beam-wave interaction is guaranteed to occur only in the output section instead of the input section. Therefore, the helix pitch of the input section is held constant (0.8014, mm), and the focus in this experiment is to optimize the helix pitch in the output section. The total length of the output section in our experimental STWT is approximately 70 mm, and it is divided into seven sections whose initial length is 10 mm.

TABLE IV  
GS-MOCSO INITIALIZATION PARAMETERS

Parameter	Value
<i>Initial cats</i>	100
<i>D (Maximum dimension)</i>	7
<i>SMP</i>	3
<i>SRD</i>	0.1
<i>CDC</i>	80%
<i>MR<sub>max</sub></i>	0.75
<i>MR<sub>min</sub></i>	0.25
<i>W</i>	0.2~0.75
<i>C</i>	2
<i>r</i>	[0,1]
<i>ε</i>	0.03
<i>G</i>	100* e <sup>-20</sup>

The pitch variation range in each section is 0.7~0.9 mm based on practical experience. Table IV shows the initialization parameters of the GS-MOCSO algorithm. Cat  $x_{i,d}$  defines a pitch distribution. The pitches in a pitch distribution set are

denoted as Pitches 4~10 and are given in mm. The total number of initial cats is 100; these represent 100 sets of pitch distributions recorded during the actual manufacturing process. The termination criterion for all algorithms is the maximum number of iterations (500). Because of the random nature of the optimization process, the experiments were all executed independently 20 times.

### C. Experiment procedures

Based on the initial parameters, the 1-D CHRISTINE code used in the GS-MOCSO algorithm can obtain the output power by solving Eq. (1). It then calculates the electronic beam efficiency, which also measures the phase shift. As a result, the two objective functions  $f_1(x)$  and  $f_2(\omega_i)$  can be evaluated. A Pareto-optimal front is obtained after the multi-objective optimization, based on the actual manufacturing requirements. After continuous optimization by GS-MOCSO, the best pitch distribution value  $x_{g,d}$  that results in the highest electronic beam efficiency and lowest phase shift is calculated. Next, the actual pitch distribution in the slow-wave structure is implemented on  $x_{g,d}$  to improve the manufacturing efficiency and reduce test costs.

The algorithm's parameters are initialized before optimization. Each cat represents a pitch distribution.  $x_{i,d}$  is the position of the  $i$ -th cat in the  $d$ -th dimension ( $1 < d < D$ ), which is the  $i$ -th pitch distribution ( $d$  is the number of sections in the helix). The cats' positions are initialized using the constant 0.8014 mm and varied within the initial range of 0.7~0.9 mm. The cat population size is 100, and the maximum number of iterations  $IT_{max}$  is 500. The GS-MOCSO parameters are set as shown in Table III. The cats are distributed among the two modes using  $MR_L$  and can be detailed as follows:

#### Seeking Mode

The parameters, including PMO, CDC, SMP, and SRD, are initialized.

1. The SMP copies of the  $i$ -th cat are produced.
2. For each cat, the CDC is determined; thus, a population of cats is generated.
3. For the entire cat population, mutation is performed according to the SRD.
4. The fitness is evaluated for the  $i$ -th cat (the  $i$ -th set of pitches) according to Eq. (18). The electronic efficiency and phase distortion are obtained by the dispersion and coupling impedance module, the 1-D CHRISTINE code module, and the phase shift module. These calculations provide the two fitness values for the  $i$ -th cat.
5. The nondominated cat positions are selected based on their fitness values, stored, and updated in the external archive.

#### Tracing Mode

1. The position  $x_{i,d}$  and velocity  $v_{i,d}$  of the  $i$ -th cat in the  $d$ -th dimension are updated by Eq. (17) to trace the targets and approach the optimum solution  $x_{g,d}$ .
2. The fitness of all cats is evaluated in the multi-objective function concerning electronic beam efficiency and nonlinear

phase distortion, where  $x_{g,d}^1$  is the best solution for the electronic beam efficiency, and  $x_{g,d}^2$  is best for phase shift.

The two objective functions collectively determine the optimal position of each cat. The weighted average method is used to evaluate the compromise values of electronic efficiency and phase shift. The expression is as follows:

$$x_{g,d} = a * x_{g,d}^1 + (1 - a) * x_{g,d}^2, \quad (19)$$

where  $x_{g,d}$  is the weighted average of  $x_{g,d}^1$  and  $x_{g,d}^2$ ,  $a \in [0,1]$ . The effects of  $x_{g,d}^1$  or  $x_{g,d}^2$  on  $x_{g,d}$  are determined as the change of  $a$ . When  $a$  has larger values, we pay more attention to improving electronic beam efficiency. When  $a$  has smaller values, we pay more attention to reducing the phase shift.

3. The contents of the archive are updated with the cats' positions, which represent a nondominated optimal solution.

4. Optimizing the gravitational search operator. Under the influence of the gravity of cats with heavier gravitational and inertial mass, the other cats exhibit a positional change in each dimension to ensure that every cat improves poor dimensional values. The new cat positions are generated as the initial population for the next iteration.

5. The seeking and tracing processes repeat until the optimization criterion is achieved. The algorithm outputs the  $x_{g,d}$  that expresses the best pitch distribution after the total optimization process is completed.

## V. EXPERIMENT AND ANALYSIS

Based on the evaluation criteria of multi-objective function, the GS-MOCSO algorithm is combined with the 1-D CHRISTINE code and applied to the slow-wave structure design to implement experiment. The experiment is to find a best pitch distribution that produces higher beam efficiency and lower phase shift.

### A. Single objective function optimization

In this paper, to verify the superiority of the multi-objective model, the GS-MOCSO algorithm first performs single-objective function optimization. We set  $f_1(x)$  as the objective function to optimize only the electronic beam efficiency and set  $f_2(\omega_i)$  as the objective function to optimize only the phase shift.

#### Improve electronic beam efficiency only

Because the first objective only improves the electronic beam efficiency, its efficiency is rapidly improved by the GS-MOCSO algorithm. The optimization curve of electronic beam efficiency is shown in Fig 5 (a), in which the x-axis represents the iteration number and the y-axis represents beam efficiency. The optimization curve rises steadily in the early stages and tends to stabilize after 5 iterations, during which the beam efficiency rises from 30% to 38.3%. Then, the curve rises steadily and finally reaches the optimum beam efficiency of 42.6% at the 18th iteration. Compared to the rated efficiency of 30% for STWT, GS-MOCSO improves efficiency by 12.6%. However, the improvement in electronic beam efficiency comes at the expense of linear

performance. The pitch distribution with optimum beam efficiency causes a phase shift of approximately  $110^\circ$ , which exceeds the phase shift range of the STWT. The phase distortion caused by the slow-wave structure design when only the electronic beam efficiency is optimized is very serious.

#### Decrease phase shift only

The optimization on only the phase shift by the proposed GS-MOCSO algorithm is shown in Fig. 5(b), in which the x-axis represents the iteration number and the y-axis represents phase shift. Because the objective function only affects the phase shift, the phase shift curve decreases gradually with the increasing iterations falling from an initial value of  $60.2^\circ$  to the optimum value of  $2.1^\circ$  and achieves convergence after only 22 iterations. However, the pitch distribution obtained by optimizing only the phase shift does not improve the electronic beam efficiency, which consistently remains at approximately 28.8%.

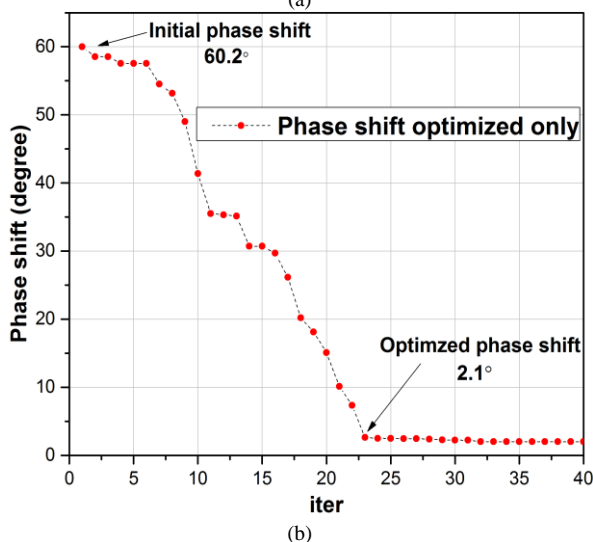
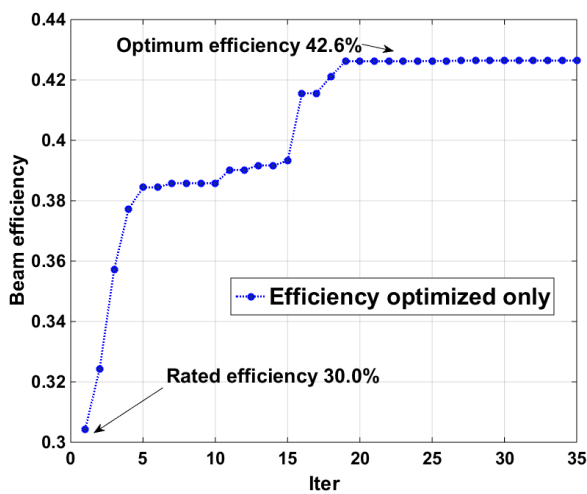


Fig 5. The optimization on electronic efficiency only (a) phase shift only (b) by the proposed GS-MOCSO algorithm

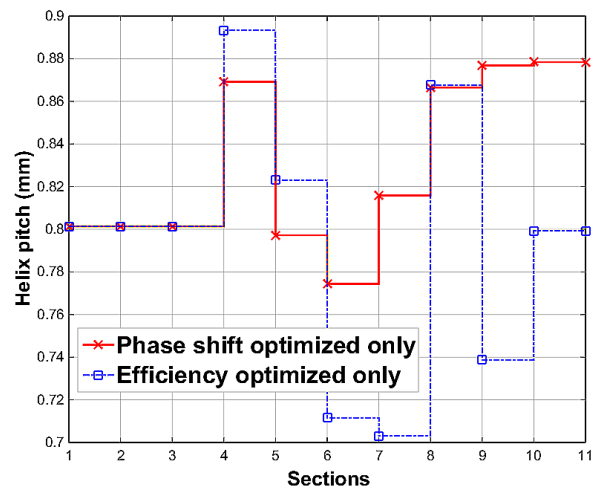


Fig. 6. Pitch distributions when only beam efficiency is optimized and only phase shift is optimized

The pitch distributions with optimal beam efficiency and optimum phase shift are shown in Fig. 6. The x-axis represents the helix section number along the STWT axis and the y-axis represents the pitch value of the corresponding section in mm. The graphed pitch distribution contains constant pitches 1~3 in the input sections and pitches 4~10 in the final seven sections of the output. The pitch distributions with optimal beam efficiency and phase shift are shown in Table VI. Based on the experimental results above, the electronic beam efficiency enhancement and the phase shift reduction are a set of incompatible objective functions. This situation requires that the proposed method must improve not only the beam efficiency but also ensure that the STWT works in a linear state and reduce its nonlinear phase distortion in the slow-wave structure design.

#### B. Multi-objective optimization

This study aimed to find a best pitch distribution that produces higher beam efficiency and lower phase shift. Therefore, multi-objective optimization was implemented to avoid finding the best position for just one of the multi-objective functions. An optimized result reflects the constrained relationship among electronic beam efficiency and phase shift.

In this experiment, we apply the proposed GS-MOCSO algorithm to the slow-wave structure design of STWT. MOCSO is used as a baseline performance comparison to evaluate the capability and versatility of GS-MOCSO. The rated beam efficiency of the STWT with constant pitch is approximately 30% and the initial phase shift is about  $60^\circ$ . The constant pitch distribution is 0.8014 in each helix section and is set as the cats' initial positions.  $a$  is 0.6, as in Eq. (18), which represents that the importance of electronic beam efficiency is slightly more important than that of phase shift reduction. The results obtained by GS-MOCSO and MOCSO from 20 independent simulations are recorded. The optimized beam efficiency and phase shift values of MOCSO and GS-MOCSO are shown in Table V and compared to the results of only beam efficiency optimization and only phase shift optimization. As shown by Fig 7, the solutions are uniformly distributed over the effective surface of the two objective functions by iterative computation. The Pareto-front curve of GS-MOCSO is clearer and more complete. By comparison, the Pareto-front curve of MOCSO

is more concentrated at the lower part of the figure and is more affected by beam efficiency. The accuracy and reliability of the GS-MOCSO algorithm is better than MOCSO for the MOP in slow-wave structure design.

A comparison of the best pitch distributions with higher beam efficiency and lower phase shift generated by the GS-MOCSO and MOCSO algorithms is shown in Fig. 8. The x-axis represents the helix section number along the axial directions, and the y-axis represents the pitch value of the corresponding helix section. The graphed pitch distribution includes the first three sections (pitch 1~3) with a constant value of 0.8014 mm and the seven output sections (pitch 4~10) with the set of best pitches on GS-MOCSO and MOCSO. The first three sections, pitches 1~3, are the input part of the slow-wave structure where the pitch remains constant because it has little impact on the electronic beam efficiency. The latter seven sections, pitches 4~10, are the output where the pitches are the optimized results from the multi-objective functions. As shown in Table V, the best pitch distribution is generated by GS-MOCSO ([0.8905, 0.8379, 0.8836, 0.8416, 0.7898, 0.8033, 0.7935] (mm)). The best beam efficiency is 40.2%, which is an improvement of 10.2% compared with the initial value. Then, the optimized phase shift is  $36.5^\circ$ , a reduction of  $23.5^\circ$  below the initial value. The GS-MOCSO effectively improves the electronic beam efficiency of STWT while ensuring the phase shift reduction, achieving the experimental goal. In contrast, the best pitch distribution achieved by MOCSO is ([0.8725, 0.8632, 0.8694, 0.8158, 0.7765, 0.7741, 0.7869] (mm)), with a best beam efficiency of 38.5% and phase shift of  $36.8^\circ$ , which are 8.5% and  $23.2^\circ$  better than their initial states, respectively.

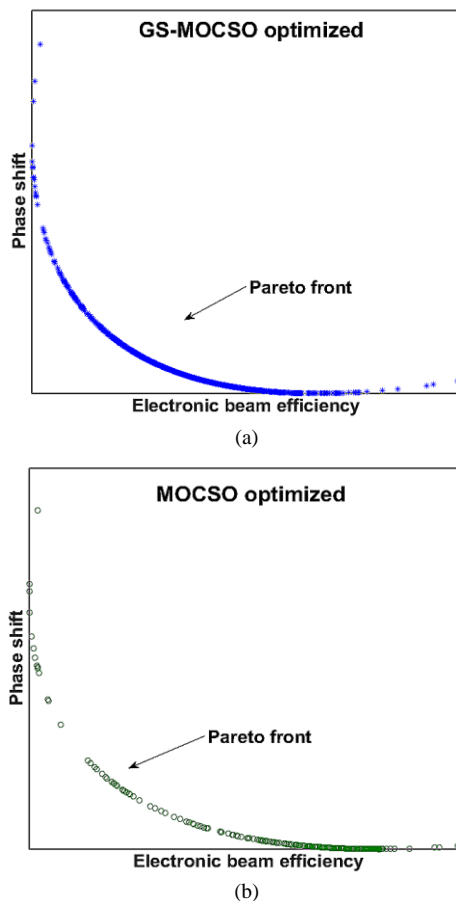


Fig 7. Pareto-front obtained with GS-MOCSO (a) and MOCSO (b) after multi-objective optimization for electronic beam efficiency and phase shift.

The phase shift reduction of the two algorithms is almost the same ( $23.5^\circ$  vs.  $23.2^\circ$ ), but the best beam efficiency of GS-MOCSO reaches 40.2%, which is significantly higher than the 38.5% achieved under MOCSO and only 2.4% lower than that achieved on beam efficiency alone. From Fig. 8, we can observe from that the pitches generated by GS-MOCSO are generally larger than those of MOCSO during the phase velocity increase section (pitches 4~7) and are lower during the phase velocity decrease section (pitch 8~10). The beam efficiency is more sensitive to pitch in the phase velocity increase section where the electron beam focus can be optimized. The phase velocity decrease section primarily performs the energy exchange between the electron beam and the electromagnetic waves, and properly reducing pitch can reduce electron beam energy loss. The results are consistent with the physical STWT mechanism. The varying amplitude of pitch value among the adjacent helix sections in the best pitch distribution optimized by GS-MOCSO is noticeably greater than that of MOCSO. Furthermore, the pitch distribution by GS-MOCSO is closer to the pitch jump change than that of MOCSO, which is closer to the gradual pitch change. The pitch jump change is more suitable for rapidly improving the output power and beam efficiency. Consequently, the optimization results of the GS-MOCSO algorithm are more consistent with the physical STWT mechanism.

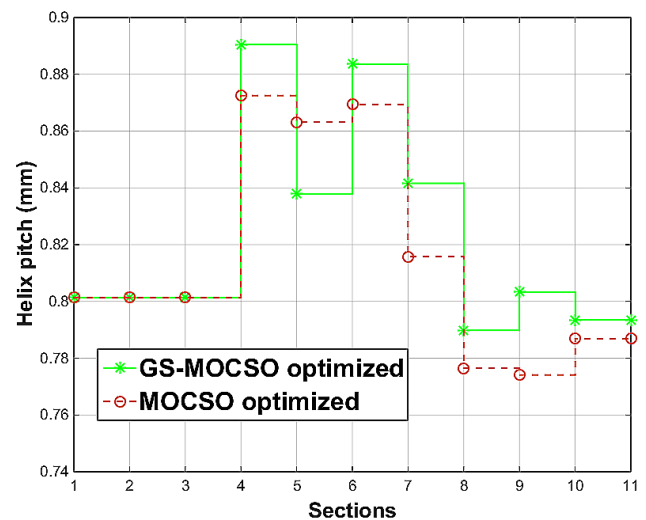


Fig 8. Comparison of the pitch distributions with best beam efficiency generated by the QPSO, MOCSO and GS-MOCSO

### C. Input power scanning

According to the best pitch distributions generated by MOCSO and GS-MOCSO, we apply the 1D-CHRISTINE code to conduct the input power scanning experiment. The varying trends of beam efficiency and phase shift with input power scanning is shown in Fig 9, where the x-axis represents input power, and the y-axis represents the electronic beam efficiency (a) and phase shift (b), respectively.

In Fig. 9(a), the beam efficiency increases as the input power increases. The maximum value reached by GS-MOCSO is 40.2% under an input power of 16 dBm. The maximum value reached by MOCSO is 38.5% under an input power of 14 dBm. However, as the input power continues to increase (to  $>20$  dBm), the electronic beam efficiency drops

significantly and falls below the rated efficiency (30%). The MOCSO curve reaches its maximum at a smaller input power compared to GS-MOCSO. The best pitch distribution obtained by MOCSO causes the STWT to enter saturation earlier and slightly lose efficiency. In addition, for the GS-MOCSO curve, the input power range is larger (16 dBm to 12 dBm) when the beam efficiency is higher than the rated value. The maximum beam efficiency is greater (40.2% compared to 38.5%), and GS-MOCSO avoids the saturation point phenomenon of STWT to a certain extent.

In Fig 9(b), the phase shifts with maximum efficiency are  $36.5^\circ$  and  $36.8^\circ$  according to the GS-MOCSO and MOCSO curves. These values are obviously better than the phase shift (60%) under a constant pitch. As the input power continues to increase, the phase shift decreases, but the beam efficiency is lower than rated value. Therefore, the input power condition is no longer applicable.

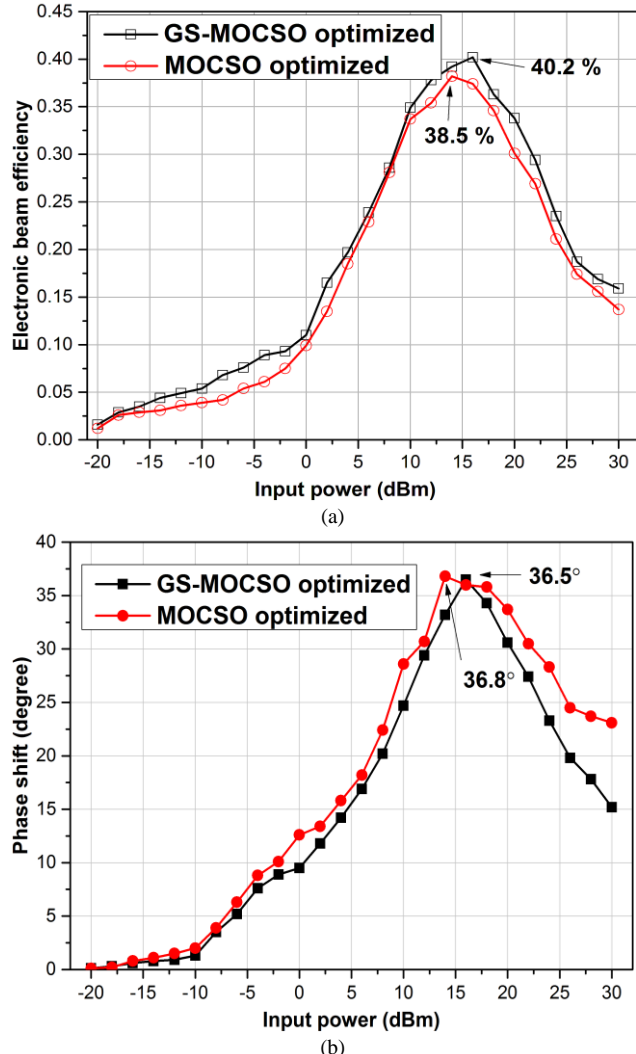


Fig 9. Curves on variation trends of electronic beam efficiency (a) and phase shift (b) with input power scanning

## VI. CONCLUSIONS

The electronic beam efficiency and phase shift of STWT directly depend on the pitch distribution in the slow-wave structure. The simultaneous efficiency improvements and phase shift suppression must be solved using multi-objective optimization. This paper proposes a multi-objective cat swarm optimization with a gravitational search operator (GS-MOCSO) that has good global search capability and

accurate convergence. The proposed optimization updates all the cats' positions and generates new positions for the next iteration based on the gravity operator. The GS-MOCSO is used to solve the MOP to improve beam efficiency and suppress phase shift. In the experimental results, the best beam efficiency of GS-MOCSO was 40.2%, which was 10.2% higher than the rated value and significantly higher than the 38.5% achieved by MOCSO. Moreover, the phase shift was  $36.5^\circ$ , which is  $23.5^\circ$  better than the value (60%) under constant pitch. In addition, the MOCSO reaches its maximum at a smaller input power than does GS-MOCSO. The best pitch distribution obtained by MOCSO causes the STWT to enter saturation earlier. In addition, the range of input power is wider (16 dBm to 12 dBm) when the efficiency is above the rated value, and the maximum beam efficiency is greater (40.2% compared to 38.5%) using GS-MOCSO. The GS-MOCSO is superior to MOCSO for the MOP of beam efficiency and phase shift. More importantly, although our research is focused on the slow-wave structure design in a STWT, GS-MOCSO can be applied to other complex multi-objective problems in the electromagnetic energy and microwave fields.

At present, these experiments results have shown that under gravitational search operator, the poor positions information of cats can interact with optimum cats (non-dominated optimal solutions) in each dimension to increase the diversity of cats and prevent falling into local optimum. But all cats' positions are updated by gravitational search operator at the end of each iteration, GS-MOCSO need more computing time than MOCSO. As future work, we will plan to further study how to deal with the computing time problem of gravitational search operator. In addition to the electronic efficiency and phase shift, there are some parameters including output power, gain, second-harmonic, third-order intermodulation and so on, we will apply the GS-MOCSO algorithm to solve more complex multi-objective optimization problems of STWT.

## ACKNOWLEDGMENT

The authors would like to thank the editors and the anonymous reviewers for helpful comments and suggestions. The corresponding author is Prof. Kewen Xia.

## REFERENCES

- [1] S. D'Agostino, F. Emma and C. Paoloni, "Accurate analysis of helix slow-wave structures," in *IEEE Transactions on Electron Devices*, vol. 45, no. 7, pp. 1605-1613, Jul 1998.
- [2] D. S. Komm, R. T. Benton, H. C. Limburg, W. L. Menninger and Xiaoling Zhai, "Advances in space TWT efficiencies," *IEEE Transactions on Electron Devices*, vol. 48, no. 1, pp. 174-176, Jan 2001.
- [3] D. K. Abe, B. Levush, T. M. Antonsen, D. R. Whaley and B. G. Danly, "Design of a linear C-band helix TWT for digital communications experiments using the CHRISTINE suite of large-signal codes," *IEEE Transactions on Plasma Science*, vol. 30, no. 3, pp. 1053-1062, Jun 2002.
- [4] M. Aloisio and P. Waller, "Analysis of helical slow-wave structures for space TWTs using 3-D electromagnetic simulators," *IEEE Transactions on Electron Devices*, vol. 52, no. 5, pp. 749-754, May 2005.
- [5] L. Xiao, X.B. Su, P.K. Liu, "Study of space charge field based on sheath helix model of TWTS". *Acta Physica Sinica*, vol. 55, no. 10, pp. 5150-5156, May 2006.

[6] Jun Sun, Bin Feng and Wenbo Xu, "Particle swarm optimization with particles having quantum behavior," *Proceedings of the 2004 Congress on Evolutionary Computation (IEEE Cat. No.04TH8753)*, 2004, pp. 325-331. Vol.1.

[7] Zhang X Y, Tang K S, Li S. "Design of Slow-Wave Structure Based on Multi-Objective Quantum Particle Swarm Optimization Algorithm with Inertia Weight", *Chinese Journal of Vacuum Science & Technology*, vol. 30, no. 6, pp. 651-656, Nov 2010.

[8] Chu S C, Tsai P, Pan J S. "Cat Swarm Optimization". *Lecture Notes in Computer Science*, vol. 12, no. 6, pp. 854-858, Aug 2006.

[9] Y. Sharafi, M. A. Khanesar and M. Teshnehlab, "Discrete binary cat swarm optimization algorithm," *The 3rd IEEE International Conference on Computer, Control and Communication (IC4)*, Karachi, 2013, pp. 1-6.

[10] G. Ram, D. Mandal, R. Kar and S. P. Ghoshal, "Cat Swarm Optimization as Applied to Time-Modulated Concentric Circular Antenna Array: Analysis and Comparison with Other Stochastic Optimization Methods," in *IEEE Transactions on Antennas and Propagation*, vol. 63, no. 9, pp. 4180-4183, Sept. 2015.

[11] B. Kumar, M. Kalra and P. Singh, "Discrete binary cat swarm optimization for scheduling workflow applications in cloud systems," *2017 3rd International Conference on Computational Intelligence & Communication Technology (CICCT)*, Ghaziabad, 2017, pp. 1-6.

[12] Pappula, Lakshman, and D. Ghosh. "Linear antenna array synthesis using cat swarm optimization." *AEU - International Journal of Electronics and Communications*, vol. 68, no. 6, pp. 540-549, May. 2014.

[13] Pappula, Lakshman, and D. Ghosh. "Synthesis of linear aperiodic array using Cauchy mutated cat swarm optimization." *AEU - International Journal of Electronics and Communications*, vol. 72, no. 3, pp. 52-64, Jan. 2017.

[14] Q. Zhu et al., "An External Archive-Guided Multiobjective Particle Swarm Optimization Algorithm," *IEEE Transactions on Cybernetics*, vol. 47, no. 9, pp. 2794-2808, 2017.

[15] Zhang, H., Yang, R., Sun, C., & Han, H. "Research on multi-aircraft cooperative suppression interference array based on an improved multiobjective particle swarm optimization algorithm." *Mathematical Problems in Engineering*, vol. 02, no. 1, pp. 1-12, 2017

[16] Pradhan, Pyari Mohan, and G. Panda. "Solving multiobjective problems using cat swarm optimization." *Expert Systems with Applications*, vol. 39, no. 3, pp. 2956-2964, Dec. 2012.

[17] Dwivedi, A. K., & Patel, R. N. "Chapter 10 – digital filter design using quantum-inspired multiobjective cat swarm optimization algorithm," *Quantum Inspired Computational Intelligence*, vol. 12, no.7, pp 327-359, 2017.

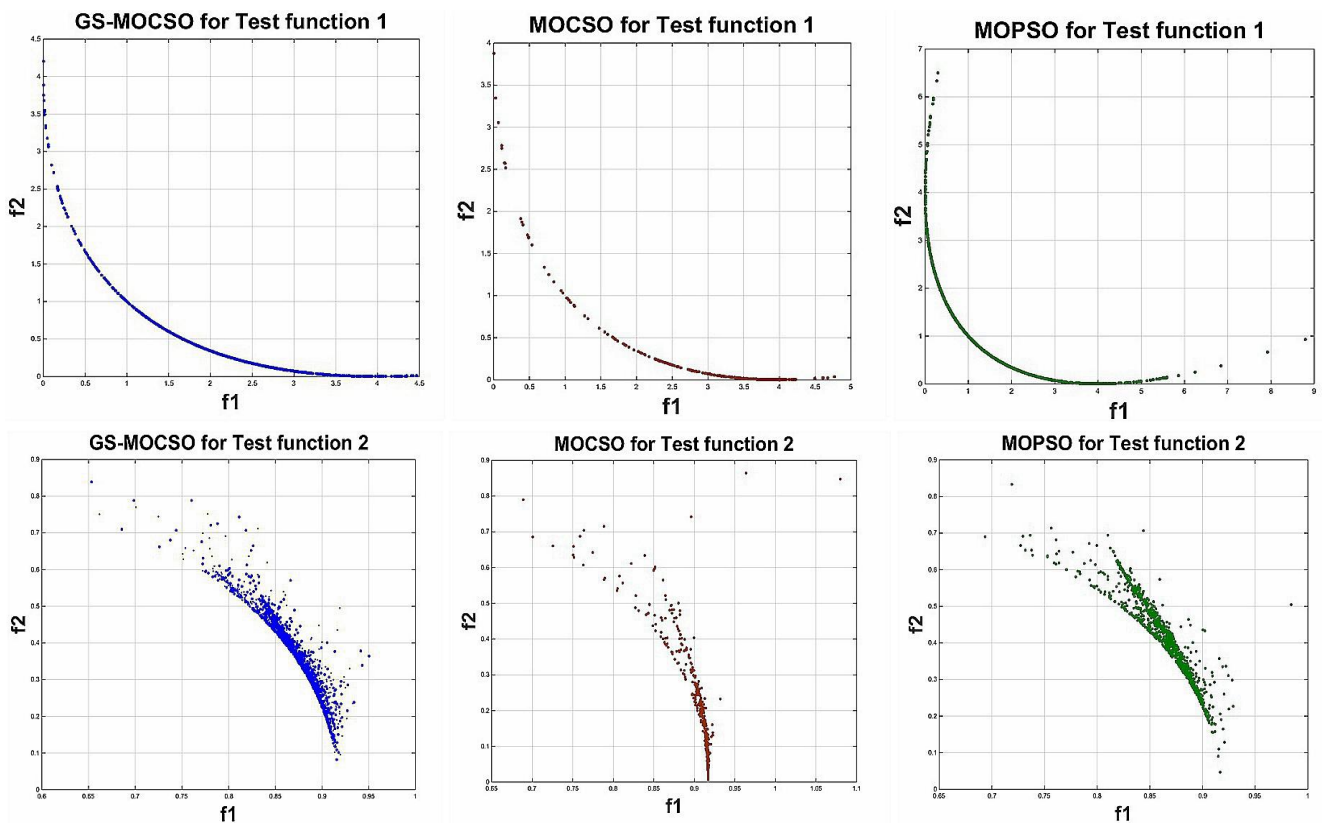
[18] C. Luo, Y. Guo, Y. Ma, C. Lv and Y. Zhang, "A non-random multi-objective cat swarm optimization algorithm based on CAT MAP," *2016 International Conference on Machine Learning and Cybernetics (ICMLC)*, Jeju, 2016, pp. 29-35.

[19] Rashedi E, Nezamabadi H, Saryzadi S. "GSA: A gravitational search algorithm". *Information Science*, vol. 179, no. 13, pp. 2232- 2248, Jun. 2009.

[20] F.s. Saeidi-Khabisi and E. Rashedi, "Fuzzy gravitational search algorithm," *2012 2nd International eConference on Computer and Knowledge Engineering (ICCKE)*, Mashhad, 2012, pp. 156-160.

[21] Xu Kang, and Dechang Pi, "Forecasting Satellite Power System Parameter Interval Based on Relevance Vector Machine with Modified Particle Swarm Optimization," *IAENG International Journal of Computer Science*, vol. 44, no.1, pp68-78, 2017

[22] Chun-Feng Wang, and Yong-Hong Zhang, "An Improved Artificial Bee Colony Algorithm for Solving Optimization Problems," *IAENG International Journal of Computer Science*, vol. 43, no.3, pp336-343, 2016



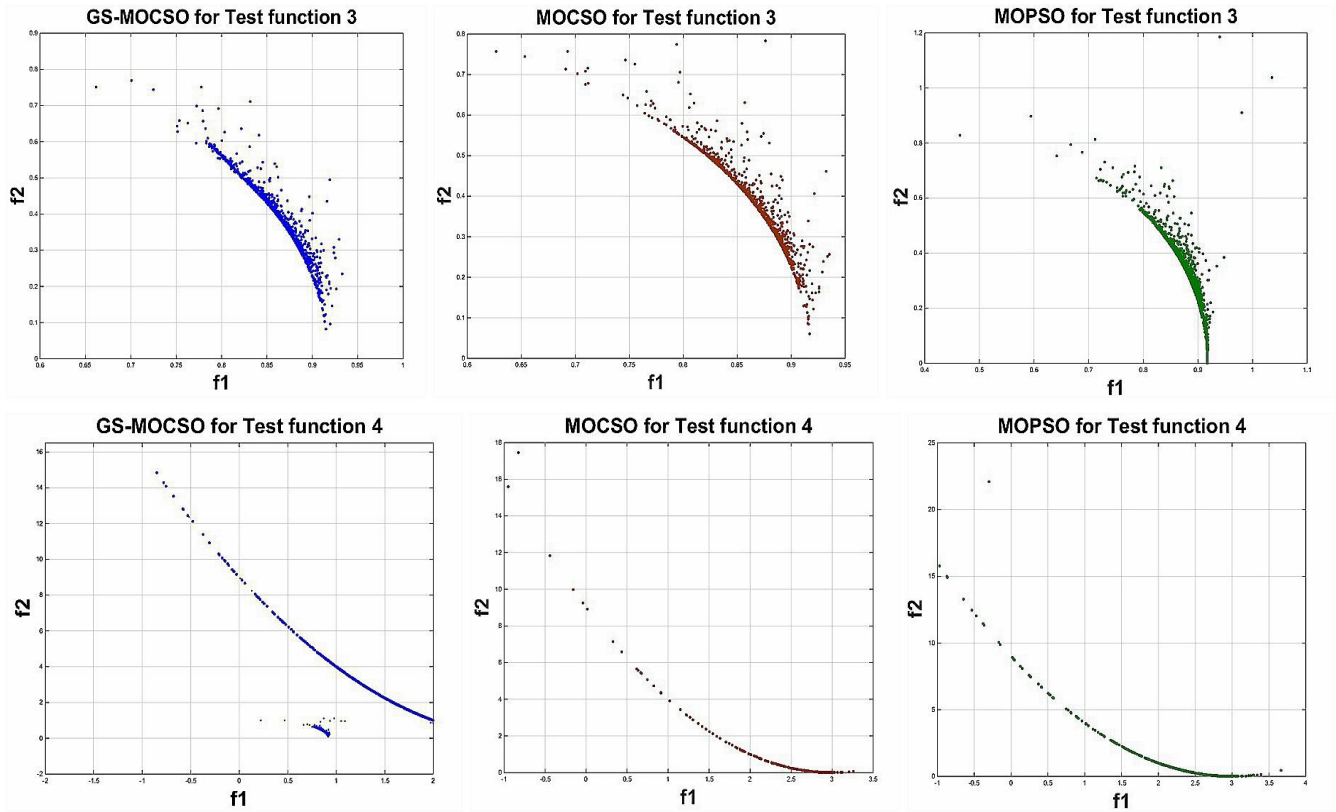


Fig 4. The diagram of test function 1~4 calculated by GS-MOCSO, MOCSO and MOPSO algorithms

TABLE V  
OUTPUT PARAMETER ON BEAM EFFICIENCY OPTIMIZED ONLY AND PHASE SHIFT OPTIMIZED ONLY

Iterations number		Iter1	Iter2	Iter3	Iter	Iter16	Iter17	Iter18	Iter19	Iter	Iter22
GS-MOCSO optimized	Beam efficiency only (%)	30.43	32.43	35.72	...	40.32	41.56	42.12	42.62	...	...
	Phase shift only (degree)	60.201	58.537	57.544	...	20.208	18.104	10.193	7.347	...	2.089

TABLE VI  
PITCH DISTRIBUTION VALUE, OPTIMIZED BEAM EFFICIENCY AND PHASE SHIFT ON SEVERAL OPTIMIZATION MODELS

Models	Pitch distribution (mm)							Optimized beam efficiency	Optimized phase shift
	Pitch 4	Pitch 5	Pitch 6	Pitch 7	Pitch 8	Pitch 9	Pitch 10		
GS-MOCSO optimized	0.8905	0.8379	0.8836	0.8416	0.7898	0.8033	0.7935	40.2%	36.5°
MOCSO optimized	0.8725	0.8632	0.8694	0.8158	0.7765	0.7741	0.7869	38.5%	36.8°
Efficiency optimized only	0.8933	0.8231	0.7116	0.7031	0.8676	0.7387	0.7993	42.6%	110°
Phase shift optimized only	0.8692	0.7972	0.7744	0.8159	0.8665	0.8768	0.8784	28.8%	2.1°